TAMPEREEN TEKNILLINEN YLIOPISTO
TAMPERE UNIVERSITY OF TECHNOLOGY

ANNA TAPANINAHO

DEVELOPMENT OF A CONDUCTIVITY MEASUREMENT METHOD DURING INSTALLMENT OF DEEP BRAIN STIMULATION ELECTRODES

Master of Science Thesis

Examiner: Professor Hannu Eskola
Examiner and subject approved by the Faculty Council on 9 August 2017

ABSTRACT

ANNA TAPANINAHO: Development of a conductivity measurement method during installment of deep brain stimulation electrodes
Tampere University of Technology
Master of Science Thesis, 46 pages
September 2017
Master's Degree Programme in Electrical Engineering
Major: Biomedical Instrumentation
Examiner: Professor Hannu Eskola

Keywords: deep brain stimulation, conductivity, impedance, resistivity, brain tissue, grey matter, white matter

The dielectric properties of brain tissue such as conductivity depend on several factors including temperature and frequency. Thus, the conductivity values obtained post-mortem from tissue samples at high frequencies do not describe properly the behavior of the conductivity at body temperature at low frequencies. The brain tissue conductivity data is scarce and most of the measurements are done from tissue samples at very high frequencies.

The primary goal of this thesis was to examine different methods used for conductivity measurement and collect brain tissue conductivity data published in 2000 or later. These methods include e.g. intracerebral technique, electrode impedance tomography and MRI-based methods. This thesis includes studies made on both living humans and animals in addition to studies conducted on post-mortem tissue samples.

The final goal of this thesis was to develop a novel conductivity measurement method during installment of deep brain stimulation electrodes. The device used is a clinician programmer used for example in deep brain stimulation, called N'Vision by Medtronic. Thus, the method measures the conductivity directly from the brain tissue. The method has it challenges, such as control of the tissue environment, but we believe that the developed method can be used in brain tissue conductivity measurement.

TIIVISTELMÄ

ANNA TAPANINAHO: Johtavuusmittausmenetelmän kehittäminen syväaivostimulaatioelektrodien asentamisen yhteydessä
Tampereen teknillinen yliopisto
Diplomityö, 46 sivua
Syyskuu 2017
Sähkötekniikan diplomi-insinöörin tutkinto-ohjelma
Pääaine: Biolääketieteen instrumentointi
Tarkastaja: professori Hannu Eskola

Avainsanat: aivokudos, harmaa aine, valkea aine, johtavuus, impedanssi, resistiivisyys, syväaivostimulaatio

Aivokudoksen dielektriset ominaisuudet kuten johtavuus riippuvat monesta tekijästä, joita ovat esim. kudoksen lämpötila ja mittauksessa käytetty taajuus. Tästä syystä, korkealla taajuudella mitatut johtavuusarvot kuoleman jälkeisistä kudosnäytteistä eivät vastaa pienellä taajuudella ruumiinlämmössä mitattuja arvoja. Aivokudoksen johtavuus data on harvassa ja suurin osa julkaisuista ovat mitanneet johtavuutta kudosnäytteistä korkeilla taajuuksilla.

Tämän diplomityön ensisijaisena tarkoituksena oli ottaa selvää johtavuusmittauksissa käytetyistä tekniikoista ja kerätä vuoden 2000 jälkeen julkaistua johtavuusdataa. Näihin tekniikoihin lukeutuu mm. aivonsisäiset metodit, impedanssitomografia ja magneettikuvaukseen perustuvat menetelmät. Tähän työhön on kerätty sekä ihmisillä että eläimillä tehtyjä tutkimuksia. Näihin lukeutuvat elävillä ja kudosnäytteillä tehdyt tutkimukset.

Tämän työn perimmäinen tavoite oli kehittää syväaivostimulaatioelektrodien asentamisen yhteydessä suoritettava johtavuusmittausmenetelmä. Menetelmässä hyödynnetään esimerkiksi syväaivostimulaatiossa käytettävää Medtronicin N'Vision ohjelmoijaa. Menetelmällä mitataan siis johtavuus suoraan elävästä aivokudoksesta, mikä tuo omat tekniset haasteensa mittauksiin. Suurena haasteena on mittausympäristön kontrollointi esimerkiksi selkäydinnesteen vuoto mittauskohtaan. Uskomme kuitenkin, että kehittämällämme mittausmenetelmällä voidaan aivokudoksen johtavuutta mitata.

PREFACE

I want to thank my examiner Hannu Eskola for his guidance and especially for his compassion and flexibility regarding the schedule of this thesis.

I also want to thank Kai Lehtimäki for introducing me the concept of DBS, Mattias Åstrom for providing me the necessary information on the measurement device and Juha Latikka for his advice.

Finally, I would like to thank my family for the support and love they have shown me during this thesis project. Special thanks go to my dad whose spirit has been right by my side and whose wisdoms I will never forget.

In Tampere, Finland on 19 September 2017

Anna Tapaninaho

TABLE OF CONTENTS

ABBREVIATIONS AND SYMBOLS

ANS	autonomic nervous system
ANT	anterior nucleus of the thalamus
C_m	membrane capacitance per unit area
CNS	central nervous system
CSF	cerebrospinal fluid
CT	computed tomography
DBS	deep brain stimulation
EEG	electroencephalography
EIT	electrode impedance tomography
F	Faraday's constant
g_t	longitudinal electrical conductivity
g_e	transversal electrical conductivity
G_m	membrane conductivity per unit area
GPe	globus pallidus externa; a basal nucleus
GPi	globus pallidus interna; a basal nucleus
MEG	magnetoencephalography
MRI	magnetic resonance imaging
P	permeability
PD	Parkinson's disease
PNS	peripheral nervous system
R	gas constant
SNS	somatic nervous system
STN	subthalamic nucleus
T	temperature
V_m	equilibrium membrane potential
V_e	extracellular potential
θ	propagation velocity of the action potential
σ_i	intracellular conductivity

1. INTRODUCTION

The conductivity of human brain tissue is important parameter in e.g. electromagnetic source imaging, electroencephalography, deep brain stimulation, electrical impedance tomography, neuronavigation and radiofrequency dosimetry. A variety of medical applications and researchers rely on conductivity values taken from standard references measured from tissue samples. However, there are several factors that affect the conductivity of the brain tissue. These include e.g. the tissue temperature, the frequency used in the measurements and the chemical composition of the sample. It should also be noted that the skull, the meninges covering the brain and the cerebrospinal fluid attenuate the signal. Thus, conductivity values obtained from tissue samples at high frequencies do not correspond to values measured in-vivo at low frequency. Moreover, values obtained from the skull surface are considerably lower than those measured intracerebrally, unless the effect of the skull and meninges is removed.

The structure of this thesis is as follows. In the background section the anatomy of the central nervous system is explained and the underlying physics of the brain conductivity is described. The concept of Deep Brain Stimulation and its applications are introduced.

The goal of this thesis was to conduct a literature review on methods used for measurement of brain tissue conductivity. This literature review concentrated on studies published in 2000 or later since Latikka (1999) has made a comprehensive review of earlier studies. These methods include e.g. intracerebral methods, electrical impedance tomography and magnetic resonance imaging. Also experiments conducted on animals and post mortem are discussed.

The conductivity values obtained from literature are tabulated and categorized according to whether they are from the whole brain or more specifically from the white matter or the grey matter in addition the conductivity of cerebrospinal fluid is also mentioned if possible. The frequency or the method used in each study is mentioned in brackets after the conductivity value.

In the method –section a novel method for measuring the brain tissue conductivity during installment of Deep Brain Stimulation electrodes is introduced. This method utilizes Medtronic's N'Vision, a clinician programmer used e.g. in deep brain stimulation. A calibration procedure for the device is designed and the calculations needed in order to obtain accurate brain tissue conductivity values are explained.

In discussion –section the pros and cons of each method, including the method designed in this thesis, are discussed and evaluated. The factors, which make it difficult to measure the brain tissue conductivity regardless of the method used, and which the future research should concentrate on, are discussed.

2. BACKGROUND

The nervous system allows us to experience our environment fully and respond to a wide range of stimuli. The nervous system is in charge of our senses and it is the conductor of movement in addition it regulates single organs and entire organ systems. In this chapter, the anatomy and histology of the nervous system and its electrical properties are explained. Previous brain tissue resistivity results from other studies are tabulated and the concept of Deep Brain Stimulation is explained.

2.1. Anatomy and histology of the nervous system

Anatomically, the nervous system is divided into central nervous system (CNS) and peripheral nervous system (PNS). The CNS includes the brain and spinal cord, whereas the PNS includes both cranial and spinal nerves. Functionally, the nervous system is divided into somatic and autonomic nervous systems, SNS and ANS respectively. The SNS includes all the somatic parts of both CNS and PNS and is in charge of all the conscious voluntary control, excluding reflex arches. The ANS consists of the autonomic parts of the CNS and PNS and regulates the activity of smooth muscle, organs and glands and it is further subdivided into sympathetic and parasympathetic division in addition to enteric division. The enteric part is in charge of the autonomic functions of the alimentary tract. (Hall 2016; Bear 2016) An overview of the nervous system is presented in Figure 1.

More precisely, the CNS is considered to have seven parts. From caudal to rostral, these parts include the *spinal cord,* the *medulla,* the *pons,* the *cerebellum,* the *midbrain,* the *diencephalon* and *the cerebrum*. The medulla, pons and midbrain form the *brainstem*. The cerebrum and diencephalon are collectively called *forebrain*, whereas the cerebellum and brainstem are called *hindbrain*. Among these structures run fluid-filled spaces called *ventricles* where the cerebrospinal fluid is formed. (Purves 2012)

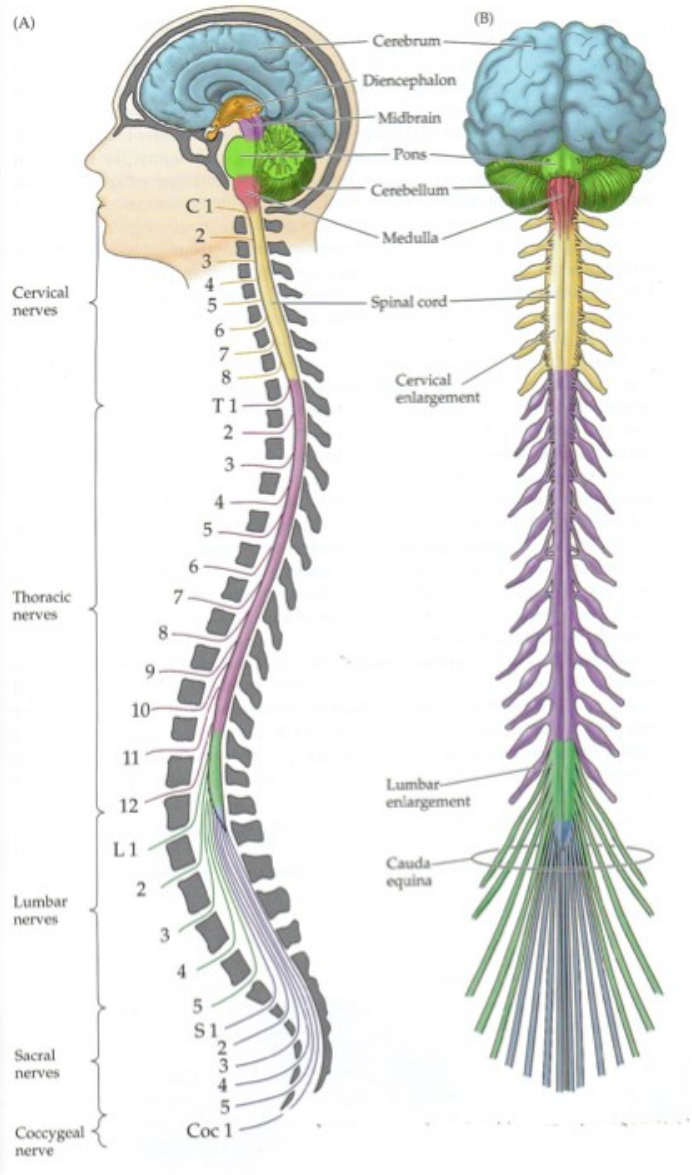

Figure 1. *Overview of the nervous system (Purves 2012)*

The two main components of nerve tissue are nerve cells aka *neurons* and supporting cells aka *neuroglial cells.* The neuron usually consists of several dendrites (neuron input), a single axon (transmission part) and a cell body, which contains the nucleus and other organelles essential in maintaining the cell (Fig. 2). The impulses are received via dendrites, which transmit the impulse towards the cell body from the periphery. The impulse proceeds away from the cell body via axon, which transmits the impulse to specialized terminal called *synapse* (output terminal). Through synapses the impulse travels from one neuron to another or e.g. to muscle cell or glandular epithelial cell. (Hall 2016; Purves 2012)

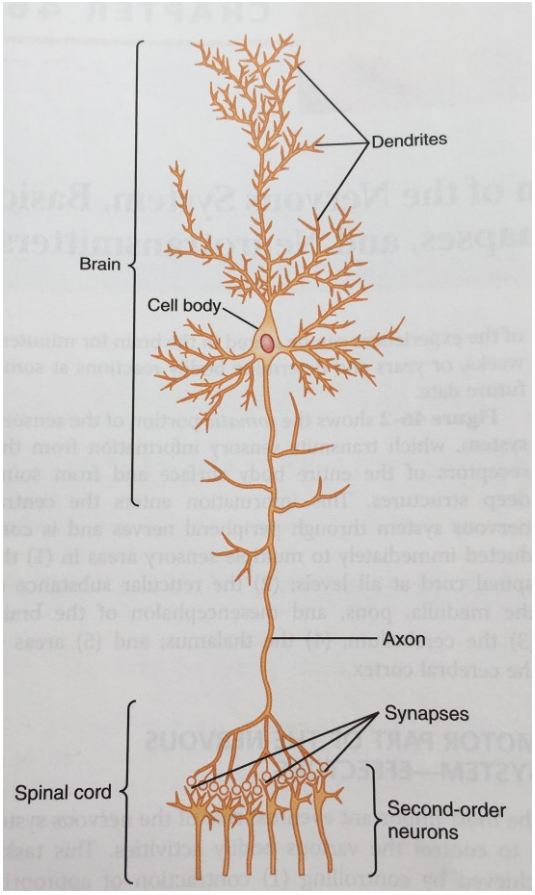

Figure 2. *The structure of a neuron in the brain. (Hall 2016)*

There are several types of neuroglial cells in both CNS and PNS. These nonconducting cells are located close to the neurons and they provide e.g. physical support, regulation of metabolism of the neuron and insulation of the nerve cell bodies and processes, thus facilitating rapid impulse transmission. (Purves 2012)

The brain matter can be separated into two types based on the colour they appear in freshly dissected brain. G*ray matter* contains the nerve cell bodies, both myelinated and unmyelinated axons, dendrites, neuroglial cells and synapses. W*hite matter*, in turn, contains only axons, neuroglial cells and blood vessels. (Ross et al. 2016)

The brain is located in the cranial cavity protected by the skull whereas the spinal cord is located in the vertebral canal and protected by the vertebrae. There are three connective tissue membranes called meninges covering the CNS (Fig. 3). The *dura mater* is the outermost membrane, underneath it lays the *aracnoidea* and the membrane attached directly on the surface of the brain and spinal cord is called *pia mater.* The space between the aracnoidea and pia mater is called *subarachnoid space* and it is filled with cerebrospinal fluid or CSF. (Purves 2012) The choroid plexuses in the lateral ventricles produce the majority of the CSF. From the lateral ventricles the CSF flows to the third ventricle through which it continues to the fourth ventricle. Through the openings in the fourth ventricle, the CSF ends up to the subarachnoid space where it enters the dural venous sinuses and bloodstream through the arachnoid granulations. (Schuenke et al. 2011)

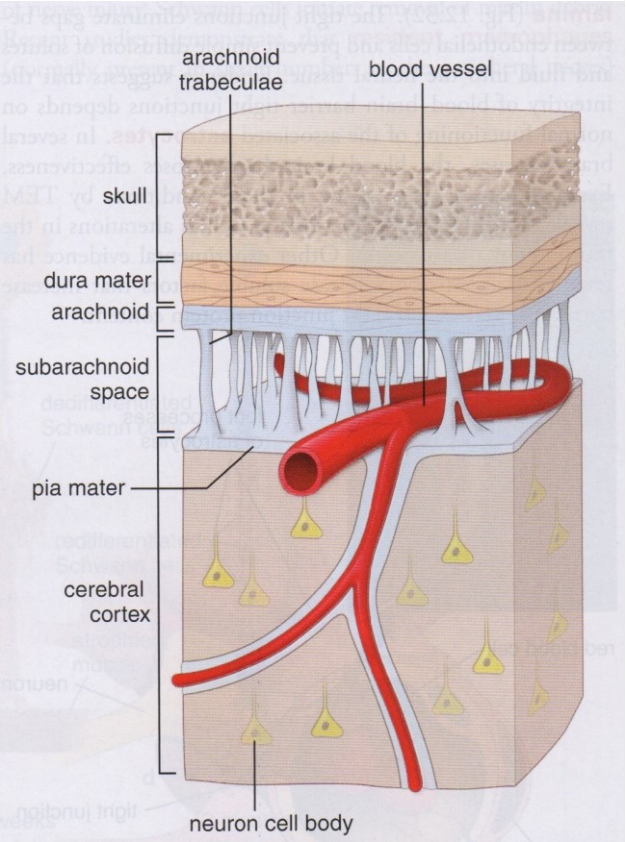

Figure 3. *The meninges. (Ross et al. 2016)*

The brain is further subdivided into cerebrum, cerebellum and brain stem. The outermost layer of the cerebrum is called *cerebral cortex*. It is 2 to 7 mm thick layer of gray matter and the majority of it is called *neocortex* and the rest *allocortex*. The main source for the EEG signals registered on the head is the neocortex, which comprises roughly 10 billion neurons with around 1000 billion connections. The cortex is largely folded, having many depressions or *sulci* and convolutions or *gyri*. Based on the locations of the sulci and gyri, the cerebrum is divided into right and left hemispheres. According to several consistent landmarks, the hemispheres are subdivided into four lobes: occipital, temporal, parietal and frontal lobe. *Central sulcu*s roughly divides the hemispheres in half, thus marking the border between the frontal and parietal lobe as seen in Figure 4. Other landmarks that divide, lobes include the *lateral fissure* between the temporal lobe and the overlying frontal and parietal lobe, and *parieto-occipital sulcus* separating the occipital lobe from the parietal and temporal lobes. (Hall 2016; Bear 2016; Schuenke et al. 2011)

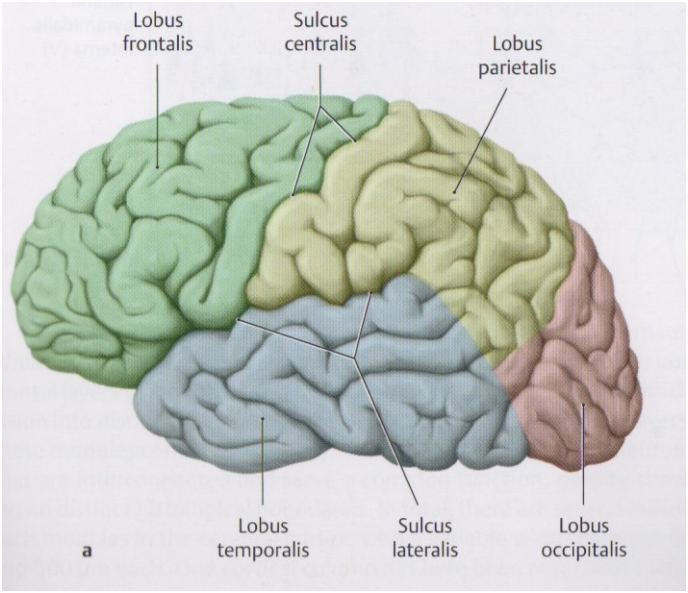

Figure 4. *Brain lobes and two of the main sulci. (Schuenke et al. 2011)*

Axons in the CNS are gathered into tracts and tracts that cross the midline of the brain, are called commissures. The biggest commissure that connects the two hemispheres is called *corpus callosum.* Corpus callosum contains axons originating from the cerebral cortex of both, right and left, hemispheres. The synapses of these axons are located in the cortex of the opposite hemisphere. (Purves 2012)

The cortex is organized vertically in six layers (lateral x-y -direction), labeled from the outermost inwards, I to VI as seen in Figure 5, and in the sensory cortex also in vertical columns with diameter of 0.5mm. The neurons in the columns no longer communicate in the z-vertical direction, but in short range in x-y -directions. The axons may be oriented laterally to neighboring areas or vertically through some of the above-mentioned layers. (Ross et al. 2016)

The molecular layer has relatively few neurons. External granular layer contains mostly stellate and small pyramidal neurons. Stellate neuron has a short axon for local information processing, whereas the axon of a small pyramidal neuron often ends within the cortex. The next few layers, external pyramidal cell layer and internal granular layer, contain small pyramidal neurons in addition to the stellate neurons in the latter layer. The internal pyramidal cell layer in turn consists of large pyramidal neurons, which have very long axons that project outside the cortex. The innermost layer, the multiform cell layer, contains neurons of varied shape and size. (Ross et al. 2016)

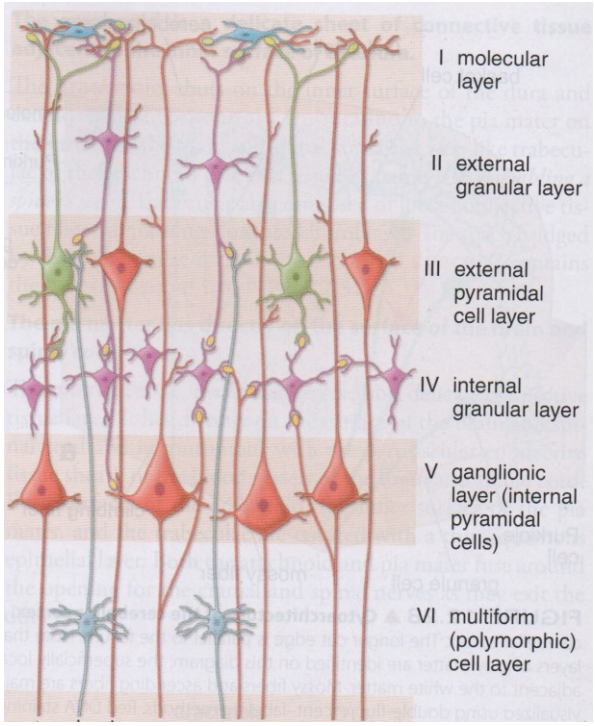

Figure 5. *The structure of the neocortex (Ross et al. 2016)*

Underneath the cortex lies a subcortical layer of white matter, where several larger grey matter structures can be distinguished. These structures are collectively called *basal ganglia* or *basal nuclei*. The largest basal ganglia include *caudate, putamen, claustrum* and *globus pallidus* (Fig. 6). Together, caudate and putamen are referred as *striatum.* The input of these ganglia originates from the cerebral cortex and the function of these structures is related to the organization and guidance of complex motor functions. Between the putamen and caudate there is an axon bundle called *capsula interna*, where the tracts from and to the cerebral cortex run. There are several smaller clusters of nerve cells ventral to the basal ganglia referred as *basal forebrain nuclei.* These nuclei modulate the neural activity in the cerebral cortex and hippocampus. *Limbic system* refers to those cortical and subcortical structures in the frontal and temporal lobes that form a medial rim of cerebrum roughly encircling the corpus callosum and diencephalon. The limbic system is associated with expression and experience of emotions in addition to regulation of visceral motor activity. The most prominent parts include the *cingulate gyrus*, the *hippocampus* and the *amyglada*. (Bear et al. 2016; Purves 2012)

The diencephalon consists of structures that include *thalamus, epithalamus* and *hypothalamus*. Thalamus forms the major component of the diencephalon and is a collection of nuclei on both sides of the third ventricle and whose primary role is to relay sensory information to the cortex from lower centers. The epithalamus consists of the *pineal gland,* which controls the circadian rhythm. The third collection of nuclei, hypothalamus, has a major role in the regulation of reproductive and homeostatic functions. Pituitary gland or *hypophysis* is a protrusion of the hypothalamus. It is an

endocrine structure comprising of two lobes, anterior or *adenohypophysis* and posterior or *neurohypophysis*. The anterior lobe secretes different kinds of hormones, whereas the posterior lobe secretes neuropeptides produced in the hypothalamus. (Bear et al. 2016; Purves 2012)

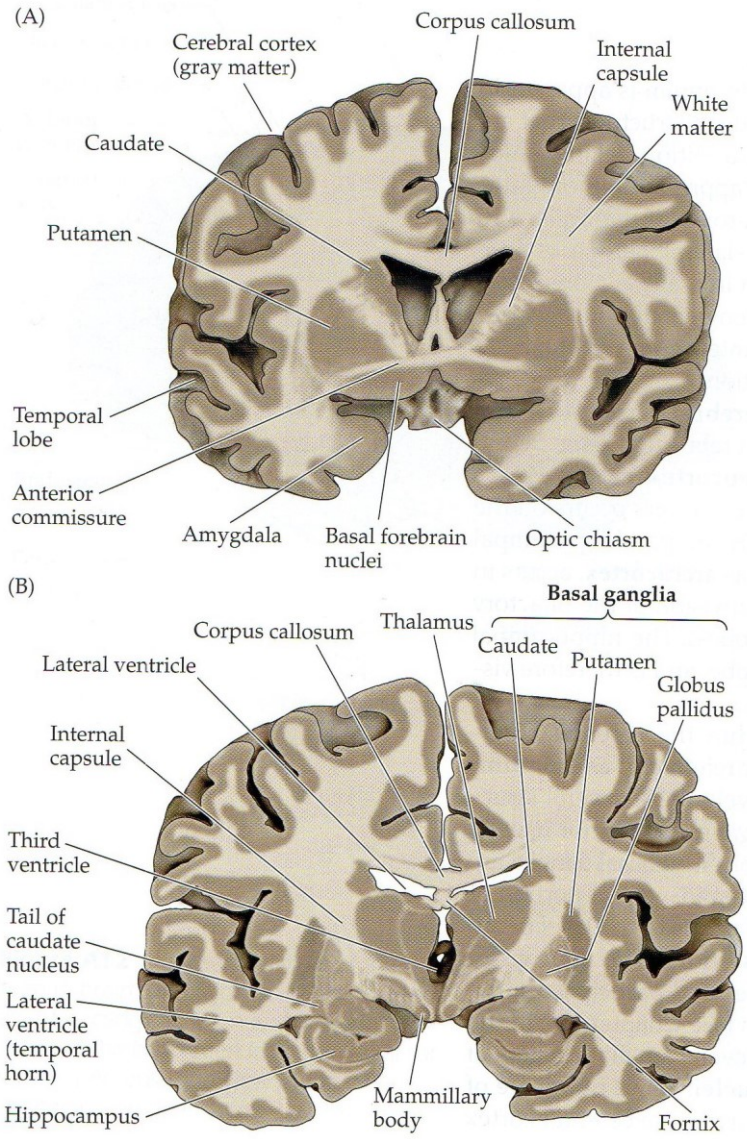

Figure 6. *The basal nuclei (Purves 2012)*

The brainstem (pons, midbrain and medulla) consists of large amount of gray matter nuclei and the surrounding white matter. The brain stem connects the brain to the spinal cord and huge amount of nerve tracts passes through and ends to the brain stem. Thus, the brain stem is an important junction station of central and peripheral nerve tracts. Overlying the brainstem is the two-hemisphere cerebellum, which is attached to the bottom of the brain with paired cerebellar peduncles. Cerebellum has an important role in e.g. motor control and maintaining the balance. Together, the brainstem and cerebellum form the hindbrain. (Bear et al. 2016; Hall 2016; Purves 2012)

2.2. The role of the basal nuclei in movement control

The basal ganglia activate before visible movement. They control the upper motor neurons and stimulate desired movements while inhibiting undesired ones. The information regulating motor functions circles a loop in the basal ganglia. There are two paths: direct for desired movements and indirect for the undesired ones. The key function in both paths is the regulation of the inhibition and activation of the thalamus. The direct path begins as the premotor cortex activation activates putamen, which in turn inhibits the globus pallidus internal. Thus, globus pallidus internal can no longer inhibit thalamus. The thalamus can now activate the primary motor cortex. This leads to activation of upper motor neuron and the desired movement is executed. The indirect path basically amplifies the inhibition of thalamus, making it unable to activate the primary motor cortex. Thus, movement is not made. (Hall 2016; Purves 2012)

Normally, these two paths operate at the same time facilitating and inhibiting movements. Dopamine, excreted by substantia nigra, plays an important role when a movement is about to be made. Dopamine has two important receptors D1 and D2. Activation of D1 excites the direct pathway, whilst D2 inhibits the indirect. As a result of the activation of the both receptors, the inhibition of globus pallidus internal increases thus releasing thalamus from the inhibition of globus pallidus internal and only the desired movements are executed. A good example of the importance of dopamine is the Parkinson's disease, in which the dopamine excretion decreases leading to increase in inhibition of thalamus. Thus, the activation of thalamus becomes more laborious and execution of movements becomes extremely difficult. (Hall 2016; Purves 2012)

2.3. Electrical properties of nerve tissue

In this chapter the electrical properties of nerve tissues in both resting and active stage are described. These properties include e.g. membrane potential, current and impedance components and action potential.

2.3.1. Resting membrane potential

The nerve cells are polarized in the steady state, what means that the interior of the nerve fiber is negatively charged with respect to the extracellular matrix. This potential difference is due to the ion pumps embedded in the cell membrane. These pumps use ATP hydrolysis as an energy source and then use this energy to transfer ions against their electrochemical gradient. The most essential ion pump is the *sodium-potassium pump* or Na^+-K^+-*ATPase*. Millions of these pumps polarize the cell to the steady state making the cell ready to react to the incoming impulses. The polarization is done by transferring three sodium ions to the extracellular matrix from the cell inferior, while

transferring two potassium ions to the opposite direction per cycle. Thus, a net current flow out of the cell of one positive ion is generated. This voltage generated is called the resting membrane potential and it is usually somewhere between -40 to -90 mV depending on the type of the neuron. (Hall 2016; Martinsen 2011)

The equilibrium membrane potential can be expressed by the following Nernst equation

$$V_m = \frac{RT}{zF} \ln \frac{c_e}{c_i}$$

where V is the equilibrium potential for any ion, R is the gas constant (8,31446 J K^{-1} mol^{-1}), T is the temperature, z is the valence of the ion, F is the Faraday's constant (96 485,3383 C/mol) and c_i is the intracellular concentration of the ion, whereas c_e the extracellular concentration of the ion. (Martinsen 2011)

When there are more than one ion species, the Goldman equation can be used. For example, with Na^+, K^+ and Cl^- the equation can be expressed as follows

$$V_m = \frac{RT}{F} \ln \frac{c_{i,Na}P_{Na} + c_{i,K}P_K + c_{e,Cl}P_{Cl}}{c_{e,Na}P_{Na} + c_{e,K}P_K + c_{i,Cl}P_{Cl}}$$

where P is the permeability (m/s). At rest the Goldman equation gives a negative voltage, which means, as mentioned earlier, the inferior of the cell is negatively charged with respect to the exterior. (Martinsen 2011)

2.3.2. Current and impedance components

Bioelectricity flows in current loops (Fig. 7), which consist of four segments. The segments are: outward and inward traversals of the cell membrane (I^1_m and I^2_m respectively) in addition to currents along the paths outside and inside the cell or cells i.e. extracellular and intracellular segments (I_e and I_i respectively). One or both the currents crossing the membrane are responsible for the energy needed for the current flow. Important ions acting as charge carriers include sodium, potassium, calcium and chloride, since these ions are able to move across the cell membrane while others are not. (Bronzino 1995)

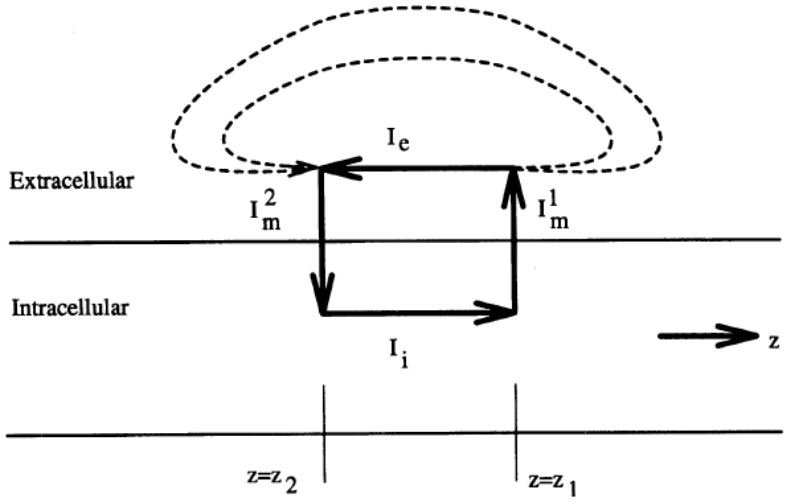

Figure 7. *An illustration of the current loop. (Bronzino 1995)*

Total membrane current I_m can be expressed as

$$I_m = I_c + I_{ion}$$

where the unit normally used for the currents is mA/cm^2. The first current component I_c depicts the charging and discharging of the membrane capacitance as follows

$$I_c = C_m \frac{\partial V_m}{\partial t}$$

where the C_m is the membrane capacitance per unit area, V_m is the transmembrane voltage and t is time. The current through the membrane is expressed with I_{ion} and it is the usually written as a sum of the charge carrier mentioned earlier, e.g.,

$$I_{ion} = I_K + I_{Na} + I_{Ca}$$

The currents of each ion is are often expressed as

$$I_{Na} = g_{Na}(V_m - E_{Na})$$

where the E_{Na} is the equilibrium potential for sodium, g_K is the conductivity of the membrane to sodium ions. It should be noted that the conductivity is not constant since it alters considerably as a function of transmembrane voltage and time. Higher conductivities are usually associated with higher conductivities. (Bronzino 1995)

The both components of the total transmembrane current differ in magnitude and direction at many sites on the membrane in addition to their effects being quite different e.g. during membrane excitation I_c usually dominates at the site of peak outward current whereas I_{ion} dominates at the site of peak inward current.

The intracellular component of the current loop flows quickly and unimpeded through the conducting medium inside the neuron. (Bronzino 1995) Plonsey and Barr (2007) introduced one-dimensional cable theory, which can be applied to the intracellular current as follows

$$I_i = -\frac{1}{r_i}\frac{\partial \phi_i}{\partial z}$$

where ϕ is the intracellular potential, r_i is the intracellular resistance per unit length, z is the axial coordinate and I_i is the longitudinal axial current per unit cross-sectional area.

The extracellular current in turn flows throughout the whole surrounding volume. Maximum current intensity is found at the membrane sites where the current enters or leaves the cell. These sites are called *sinks* and *sources* respectively. The dashed lines in Figure 7 depict how the extracellular currents extend to a wider range when the space surrounding a single nerve is not confined. According to Plonsey and Barr (2007), the direction and magnitude of the extracellular currents can be obtained with the following Poisson's equation

$$\nabla^2 \phi_e = -\frac{I_v}{\sigma_e} = -\frac{\nabla \cdot \vec{J}}{\sigma_e}$$

where the I_v is the volume density of the sources (sinks being negative sources), J is the current density and σ_e is the conductivity of the extracellular medium. The $\nabla \cdot \vec{J}$ taking on nonzero values represent the movement of the currents across the membrane from intracellular to extracellular volume, where they emerge from sources or vanish into sinks.

2.3.3. Membrane polarization and action potential

Embedded on the cell membrane there are selective ion channels constructed of proteins. These channels are closed during the resting state but they can be opened by a voltage change or binding of a ligand. The opening of the ion channels leads to an ion flow according to their electrochemical gradient, thus altering the potential difference across the cell membrane and creating an action potential (Figure 8) and depolarization of the cell. This mechanism enables the transmission of electrical signals i.e. action potentials over great distances. (Hall 2016; Martinsen 2011)

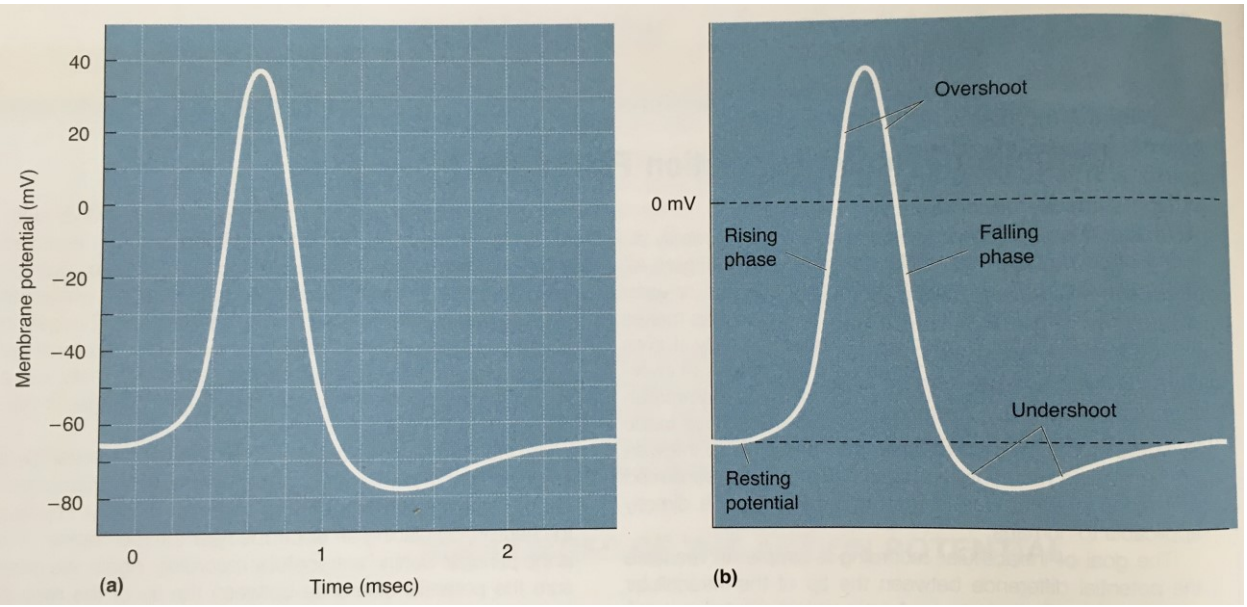

Figure 8. *a) An action potential measured by an oscilloscope b) the phases of the action potential (Bear et al. 2016)*

The action potential can be divided into three phases: depolarization (rising phase), repolarization (falling phase) and hyperpolarization (undershoot) as seen in Figure 8. After a certain threshold level is exceeded, the voltage gated sodium channels open and sodium flows into the cell leading to depolarization. The voltage rises above zero and reaches its maximum value. The sodium channels close, whereas the slower potassium channels open. Potassium ions flow outside the cell thus, decreasing the membrane potential below the resting membrane potential (hyperpolarization). During this refractory period the potential is below the resting potential making the neuron unable to get depolarized unless there is an exceptionally powerful stimulus. As a result the ion distribution is now reversed: sodium is inside the cell whereas potassium is outside. To correct this situation, the earlier discussed Na^+-K^+-ATPase returns sodium ions from inside the cell to the, while transferring potassium back inside making the neuron able to polarize when new stimulus arrives. (Hall 2016; Martinsen 2011)

The propagation velocity θ of the action potential can be expressed as

$$\theta = \sqrt{\frac{Ka}{2R_i}}$$

where R_i is the specific resistance of the intracellular medium, a is the radius of the fiber and K is a constant determined by the membrane potentials. The extracellular resistance is assumed relatively low. The velocity is proportional to the square root of the fiber radius i.e. the larger the fiber, the higher the velocity. This property is exploited in nerve tracts where the high velocity is essential e.g. proprioceptors of skeletal muscle that relay information about the position and movement of the muscle. (Bronzino 1995)

2.3.4. Conductivity of nerve tissue

The potential distribution throughout a volume conductor ϕ (V) can be assumed quasistatic in bioelectric phenomena, since the potential distribution often changes slowly enough. This way the inductive and capacitive effects and the finite speed of electromagnetic radiation can be ignored. This approximation is accurate for frequencies above 100 kHz. Under these conditions, the continuity equation

$$\nabla \cdot J = S$$

states that the divergence $\nabla \cdot$ of current density J (A/m^2) is equal to endogenous or applied source of electrical current S (A/m^3). (Bronzino 1995) According to Ohm's law, the current density of a volume conductor is linearly related to electric field (V/m) as follows

$$J = gE$$

where g is the electrical conductivity of the tissue (S/m). (Bronzino 1995) The electric field is then related to the potential gradient:

$$E = -\nabla\phi.$$

Fricke (1924) introduced the following mathematical formula for the electric conductivity of a suspension of homogenous spheroids

$$\frac{\frac{k}{k_1} - 1}{\frac{k}{k_1} + x} = \rho \frac{\frac{k_2}{k_1} - 1}{\frac{k_2}{k_1} + x},$$

where k is the specific conductivity of the suspension, k_1 is the specific conductivity of the suspending medium, k_2 is the specific conductivity of the suspended spheroids, ρ is the volume concentration of the suspended spheroid, x is a function of the ratio k_2/k_1 and the ratio a/b of the axis symmetry of the spheroids to the other axis.

Cole (1968) introduced the earliest model describing the effective electrical conductivity of biological tissues. The model consists of suspension of cells in saline solution, which constitutes the interstitial space having the conductivity σ_e. The conducting fluid inside the cell in turn constitutes the intracellular space having the conductivity σ_i. A schematic diagram and an equivalent circuit of the model are presented in Figure 9.

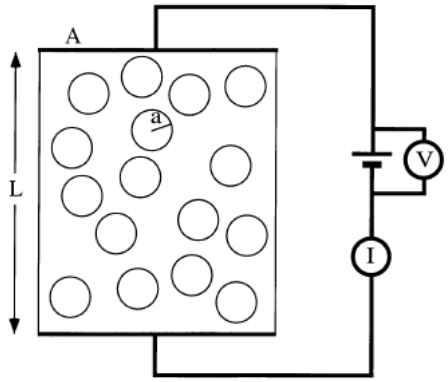

Figure 9. *A suspension of cells as a schematic diagram, where a is the radius of a cell. (Bronzino 1995)*

Between the interstitial space and the intracellular space there is a membrane with conductivity per unit area G_m (S/m^2) along with capacitance per unit area C_m (F/m^2). The parameter describing how tightly the cells are packed together is called the intracellular volume fraction or *f*, which is dimensionless and can range from 0 to 1. In case of irregularly shaped cells surface-to-volume-ratio is more convenient to use than simply radius of the cell. The surface-to-volume-ratio for spherical cells is defined as 3f/a. (Cole 1968)

In order to define the effective conductivity *g* of the cell suspension, the suspension can be placed in a cylindrical tube, having length *L* and cross-sectional area *A*. (Bronzino 1995) When DC potential difference is applied across the two ends of the cylinder, the strength of the electric field can be expressed as

$$\frac{V}{L}.$$

The total current *I* is then measured and the effective conductivity can be obtained from the following equation

$$g = \frac{I * L}{V * A}.$$

The effective conductivity *g* of a suspension of insulating spheres placed in a saline solution, having conductivity σ_e, for DC fields can be expressed as (Bronzino 1995)

$$g = \frac{2(1-f)}{2+f}\sigma_e.$$

An equivalent electric circuit of the effective conductivity of the cell suspension is presented in Figure 10.

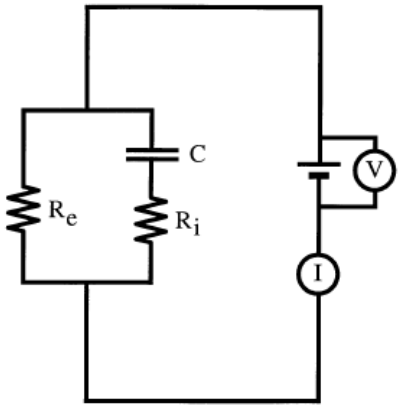

Figure 10. *An equivalent electric circuit of the effective conductivity of the cell suspension, where C is the effective membrane capacitance, R_e is the effective resistance to current passing entirely through the interstitial space, and R_i is the effective resistance to current passing into the intracellular space. (Bronzino 1995)*

The capacitance of the cell membrane is about 0.01 F/m^2. This brings the frequency dependency into the electrical conductivity. (Bronzino 1995) At low frequencies, the electrical conductivity is approximated by the previous equation, since all the current is confined to the interstitial space. At high frequencies, the capacitance shunts current across the membrane. Thus, the conductivity returns to being resistive as follows

$$g = \frac{2(1-f)\sigma_e + (1+2f)\sigma_i}{(2+f)\sigma_e + (1-f)\sigma_i}\sigma_e.$$

At intermediate frequencies, the membrane capacitance effects considerably on the effective conductivity, hence the conductivity has both real and imaginary parts. The previous equation still stands, however the conductivity of the intercellular space must be replaced with σ_i^* which is expressed as

$$\sigma_i^* = \frac{\sigma_i * Y_m * a}{\sigma_i + Y_m * a},$$

where

$$Y_m = G_m + i * \omega * C_m.$$

Due to its anisotropic nature, the nerve tissue is best approximated as a suspension of fibers. In case of fibers the effective electrical conductivity can be divided into two components: longitudinal i.e. parallel to to fibers, and transversal i.e. perpendicular to the fibers, or g_L and g_T respectively. When the electric field is perpendicular to the direction of the fibers, the tissue is better approximated as a cell suspension placed in saline solution, thus the transversal effective conductivity can be expressed as

$$g_T = \frac{(1-f)\sigma_e + (1+f)\sigma_i^*}{(1+f)\sigma_e + (1-f)\sigma_i^*}\sigma_e,$$

where σ_i is intracellular conductivity, σ_e is the conductivity of the saline solution with intracellular volume fraction f. (Bronzino 1995) When the electric field is parallel to the fibers, using cable theory (Plonsey 2007) the longitudinal effective conductivity can be derived. The g_L depends on the length of the tissue sample. A single nerve fiber can be modeled with the circuit shown in Figure 11.

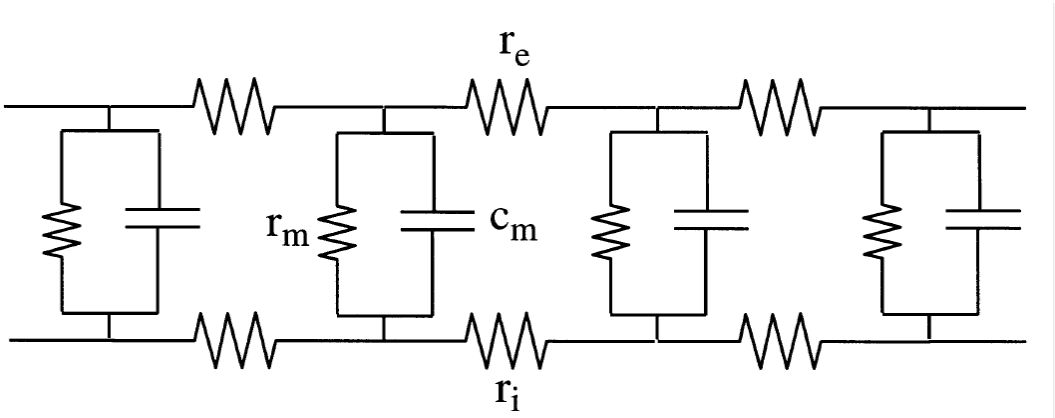

Figure 11. *An electrical circuit of a one-dimensional nerve fiber, where r_i is the intracellular and r_e the extracellular resistance per unit length (Ω/m), r_m is the membrane resistance times unit length (Ωm) and c_m is the membrane capacitance per unit length (F/m). (Bronzino 1995)*

The cable equation gives the transmembrane potential V_m as

$$\lambda^2 \frac{\partial^2 V_m}{\partial x^2} = \tau \frac{\partial V_m}{\partial t} + V_m,$$

where τ is the time constant, $r_m c_m$ and λ is the length constant $\sqrt{\frac{r_m}{r_i + r_e}}$. The solution of the cable equation for a truncated fiber with sealed ends and with a steady-state current I (A) applied to the extracellular space at one end and removed from the other, is

$$V_m = I * r_e * \lambda \frac{\sinh\left(\frac{x}{\lambda}\right)}{\cosh\left(\frac{L}{2\lambda}\right)},$$

where L is the length of the fiber and the origin of the x-axis is at the midpoint between electrodes. (Bronzino 1995) In order to calculate the voltage drop between the electrodes ΔV_e, the extracellular potential V_e can be evaluated. V_e consists of two terms, one is proportional to x and the other is $\frac{r_e}{r_e + r_i} * V_m$. Thus ΔV_e can be expressed as

$$\Delta V_e = \frac{r_e r_i}{r_e + r_i} * I * \left[L + \frac{r_e}{r_i} * 2\lambda * \tanh\left(\frac{L}{2\lambda}\right)\right].$$

If L is very large compared to λ, the abovementioned equation reduces to

$$\Delta V_e = \frac{r_e r_i}{r_e + r_i} * I * L \qquad L \gg \lambda,$$

thus the combination of extracellular and intracellular resistances becomes the main factor. In turn, if L is very small in comparison to λ, the voltage drop becomes

$$\Delta V_e = r_e * I * L \qquad L \ll \lambda$$

Thus now the main factor is the extracellular resistance. To eliminate the sample length, the effective longitudinal conductivity can be expressed in terms of spatial frequency k (rad/m) as follows

$$g_L = \frac{(1-f)\sigma_e + f\sigma_i}{1 + \frac{f\sigma_i}{(1-f)\sigma_e} \frac{1}{1 + \left(\frac{1}{\lambda k}\right)^2}}.$$

If kλ << 1, g_L reduces to $(1-f)\sigma_e + f\sigma_i$, in turn if kλ >> 1 the equation reduces to $(1-f)\sigma_e$, meaning that the current is confined to the interstitial space. Thereby the $1/k$ acts the same way as L in those equations in case of the voltage drop describer earlier. By defining λ in terms of Y_m instead of G_m, the equation ofor effective longitudinal conductivity can be applied to all temporal frequencies. (Bronzino 1995)

The variation of conductivity and permittivity with frequency is called dispersion. α – dispersion occurs at low frequencies and it is due to the counterion polarization along the cell membranes, the sarcoplasmic reticulum in muscle tissue and channel proteins on the cell membranes. β –dispersion occurs in the range of 0.1 – 10 MHz and it is due to the poorly conducting membranes between the cytoplasm and the extracellular space. The γ –dispersion occurs as a result of polarization of water molecules in the gigahertz region. (Schwan 1994) The behavior of the conductivity and permittivity in these dispersion regions is depicted in Figure 12.

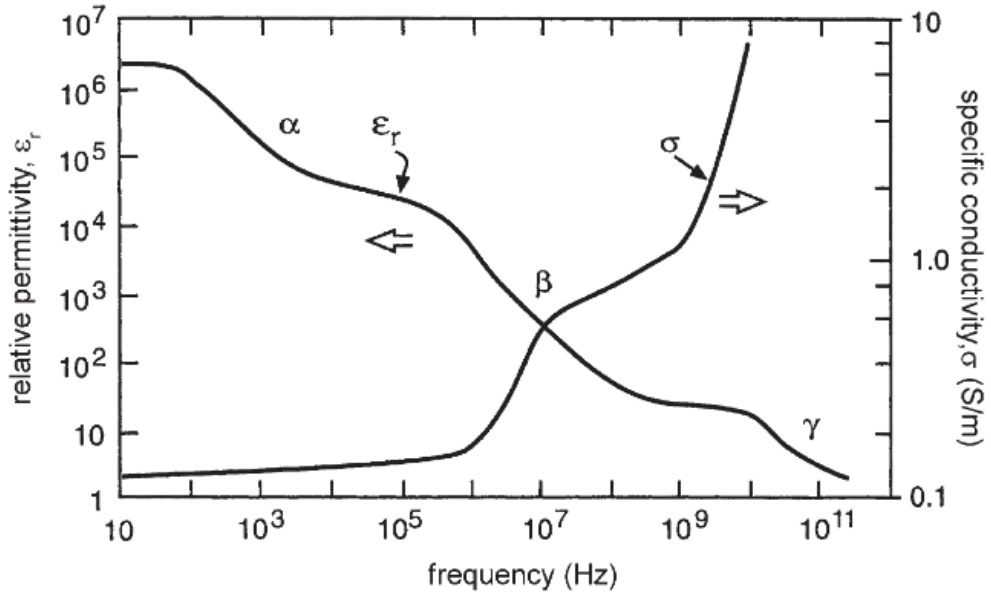

Figure 12. *Typical frequency dependence of conductivity and complex permittivity of heterogeneous material e.g. biological tissue. (Reilly 1992)*

Since the conductivity is frequency dependent, so is the tissue impedance. At low frequencies of applied current the conduction is only through the extracellular space since the current cannot cross the membrane, whereas at high frequencies the membrane act as a capacitor allowing the current to pass. Cole and Cole (1941) introduced a model of bulk tissue impedance based on the idea of the membranes acting as capacitors. As such, the model is too simple; since a large interconnected modules of this form would represent an actual tissue sample better. However, the model fits experimental data when the components are made a power function of the applied frequency ω. Thus, the tissue impedance as a function of frequency can be described reasonably well with the following equation

$$Z = Z_\infty + \frac{Z_0 - Z_\infty}{1 + \left(j\frac{f}{f_c}\right)^\alpha}$$

where Z_0 and Z_∞ are the (complex) limiting values of tissue impedance at low and high frequency and f_c is a characteristic frequency. α depends on the tissue and allows for the frequency dependency of the components of the model. (Bronzino 1995)

2.4. Deep Brain Stimulation

Deep brain stimulation (DBS) involves the surgical placement of a thin lead with four electrodes into a carefully selected brain region in either one or both brain hemispheres. The lead is connected to a pacemaker-like device or *neurostimulator* implanted below the collarbone as seen in Figure 13. The neurostimulator generates electrical pulses that

are transmitted to the target via the lead. The settings of the neurostimulator such as the number of electrodes and their combination, pulse width and amplitude etc. are all adjustable i.e. the stimulation can be tailored to meet the individual needs of each patient. DBS is used as a treatment for neurological disorders such as essential tremor, dystonia, Parkinson's disease and epilepsy.

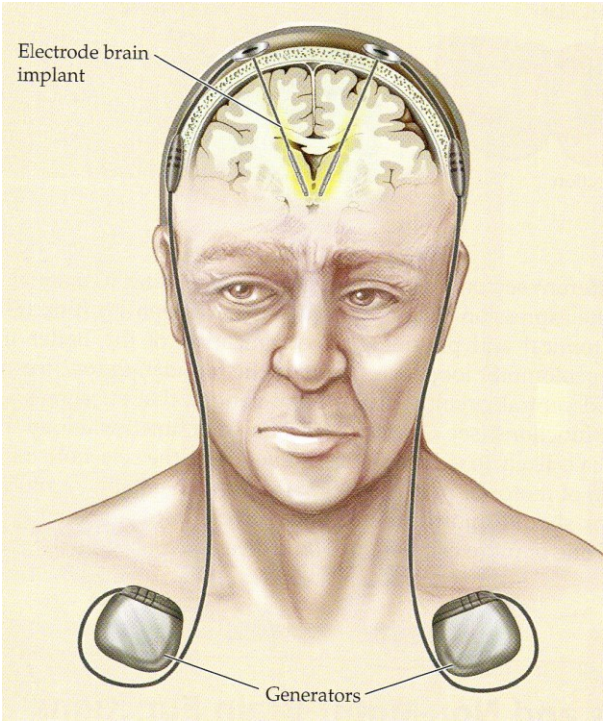

Figure 13. *Illustration of a patient with implanted DBS device. (Purves 2012)*

DBS does not destroy the brain tissue and the implantation is reversible, however there is 1-3 % risk of cerebral hemorrhage and 2-25% risk of an infection. (Siddiqui et al. 2008). The most common side effect of DBS is dysarthria, which can be alleviated by programming the stimulator. (Pekkonen 2013)

The specific target is located using stereotactic (3-dimensional) imaging techniques: X-ray, magnetic resonance imaging (MRI) or computed tomography (CT). A stereotactic frame is mounted on the patient's head in order to keep the head still after which a special hardware with the obtained coordinates are adjusted on the frame. The electrodes are implanted through a small drilling hole through a special hardware. (Pekkonen 2013; Siddiqui et al. 2008)

2.4.1. Parkinson's disease

DBS is used in advanced Parkinson's disease (PD) if conventional medications do not offer satisfactory response to the motor symptoms. DBS only eases the symptoms and improves the quality of life, therefore it is not a curative treatment and it does not stop the progression of the disease.

The most common target nucleus in treatment of PD is the subthalamic nucleus (STN) as seen in Figure 14. Other option is the globus pallidus interna (GPi). By stimulating the STN it is possible to reduce the medication, which is not possible by stimulating the GPi. Stimulation of thalamus is an option if tremor is the only symptom. (Follet 2010)

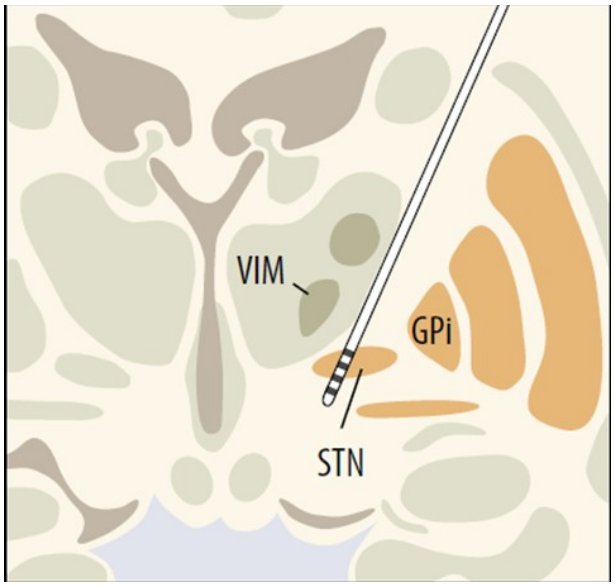

Figure 14. *The target nuclei used in Parkinson's disease. (Pekkonen 2013)*

In PD the stimulation voltage is usually around 2-5 volts. If the increase of voltage causes side effects, the pulse width and frequency can be adjusted instead. The most commonly used pulse width and frequency in PD are 60 µs and 130 Hz respectively. (Pekkonen 2013)

The mechanism of DBS is still unclear at cellular level. Animal testing have shown that activation and inhibition of neurons during STN stimulation depends on the frequency of the stimulation. High frequency has an inhibitory effect, whereas low frequency activates the neurons. The stimulation also causes changes in the oscillation of neuronal networks. These changes seem to correlate with clinical responses e.g. the STN – stimulation seems to reduce the abnormally increased betaoscillation in PD. (Krack et al. 2010)

2.4.2. Essential tremor

DBS treatment is considered if the medication does not relieve the tremor adequately. The target is the ventral intermediate nucleus of the thalamus. Due to its fast response, long at least seven years treatment efficacy (Lyons & Pahwa 2008) and fewer side effects, the DBS has superseded the previous treatment method thalamotomy i.e. the ablation of thalamus. The stimulus parameters used in essential tremor are similar to those used in PD. (Pekkonen 2013)

2.4.3. Dystonia

Primary generalized dystonia and cervical dystonia can be alleviated with DBS if the medication does not provide sufficient results (Vidailhet et al. 2008; Bronte-Stewart et al. 2011). In treatment of dystonia a wider pulse and a higher current than in PD is used to stimulate the GPi. The response to the treatment can take as long as a year. The symptoms alleviate on around 50% of the patients suffering from primary dystonia and for patients with cervical dystonia the percentage is 50 - 90%. (Vidailhet et al. 2008)

2.4.4. Epilepsy

Around 30 % of the people suffering from epilepsy do not get sufficient response to medication and the surgical removal of the epileptogenic zone is not an option for most of these patients, thus DBS is becoming a great solution for patients with refractory epilepsy. (Pekkonen 2013) According to Fischer et al. (2010) in two-year follow-up of 110 patients, who received stimulation to the anterior nucleus of the thalamus (ANT), the amount of seizures decreased by at least 50 % in 54 % of the patients. The ANT stimulation is believed to either inhibit or interfere with the epileptic nerve network. This leads to prevention of generation, propagation or generalization of the epileptic eruption (Hartikainen 2015). At the moment, Tampere University Hospital or Tays treats more epilepsy patients with DBS than any other hospital in the world. The first DBS surgeries at Tays were conducted in 2010. The results have been so remarkable that Tays has become an international DBS education center. (Tays website)

2.4.5. Alzheimer

The effect of DBS on memory was discovered by accident, when a patient underwent stimulation of hypothalamus to treat his extreme obesity. The patient had flashbacks of earlier events during stimulation and simultaneously EEG showed activation of the medial temporal lobe. (Hamani ym. 2008)

2.4.6. Other possible uses of DBS

Studies are currently being conducted on whether DBS could help patients with cluster headache, OCD, depression, obesity, restless legs -syndrome and camptocormia also known as bent spine syndrome (Lyons 2011).

2.5. Current methods for brain impedance measurement

In the following section the methods used for impedance measurements found in literature are described. Since Latikka (1999) has made a comprehensive table of studies conducted before the year 2000 in his MSc thesis, this thesis concentrated on studies

published in 2000 and later. The results of the studies are listed in Table 2 and the pros and cons of the studies are discussed later in the Discussion chapter.

2.5.1. Intracerebral methods

Latikka et al. (2001) measured brain tissue impedances from nine living patients. The measurements were performed during actual brain surgeries such as tumor removal. They used a commercially available pain treatment equipment (FL Fischer Neuro N50) with a monopolar needle electrode. Measurements were performed with a sinusoidal current of 2 μA and 50 kHz. The measurement equipment was calibrated with series of resistors and salty liquids with the aid of a multimeter and a conductivity meter in the TUT chemistry laboratory. The mean resistivities were 3.51 Ωm and 3.91 Ωm for grey matter and white matter respectively.

Koessler et al. (2017) measured the conductivity of the brain tissue in body temperature in-vivo. They used a radiofrequency generator and injected focal electrical currents at 50 kHz through intracerebral multicontact electrodes on 15 epileptic patients with mean age of 28 years. The obtained conductivity values were 0.26 S/m for grey matter and 0.19 S/m for white matter or 3.78 Ωm and 5.24 Ωm respectively. Koessler et al. also discovered that healthy grey matter had lower conductivity values than epileptogenic zone within grey matter (0.29 S/m or 3.45 Ωm), even when MRI showed no visible epileptogenic zone. Their study showed no correlation between brain tissue impedance and the age of the patient.

2.5.2. Electrical Impedance Tomography

Electrical impedance tomography or EIT is a noninvasive and radiation-free medical imaging technique for measuring the changes in tissue impedance. In 1978 Henderson et al. introduced an impedance camera, which generated electrical impedance images of the thorax. Barber et al. (1984) presented the first practical design for EIT system and published the first tomogram of a human forearm.

The principle of EIT is that a small alternating current, typically 5 mA at 20 Hz – 1 MHz, is injected into the body through electrodes on the skin and the resulting voltages are then measured at the skin surface with different set of electrodes. During EIT measurement the location of current injection and voltage measurement around the body plane are constantly rotated in order to become independent of electrode and skin impedances. For instance, lung function monitoring is usually carried out by placing 16 electrodes around the thorax. The most popular electrode configuration is referred as *adjacent drive configuration*, where the current is injected to the tissue via two neighboring electrodes, while rest of the electrode pairs measure the voltage differences. Each of the electrode pair take turns injecting the current while the others measure the voltage difference as seen in Figure 15. After one round a single frame of data is

gathered. This 16-electrode system takes total of 280 voltage measurements for one frame of data. A map or image representing the impedance changes across the plane of interest is then produced by processing the voltage measurements. The typical speed is around 30 to 50 frames per second, thus continuous monitoring of physiological changes is also possible. (Bayford 2012; Leonhardt & Lachmann 2012)

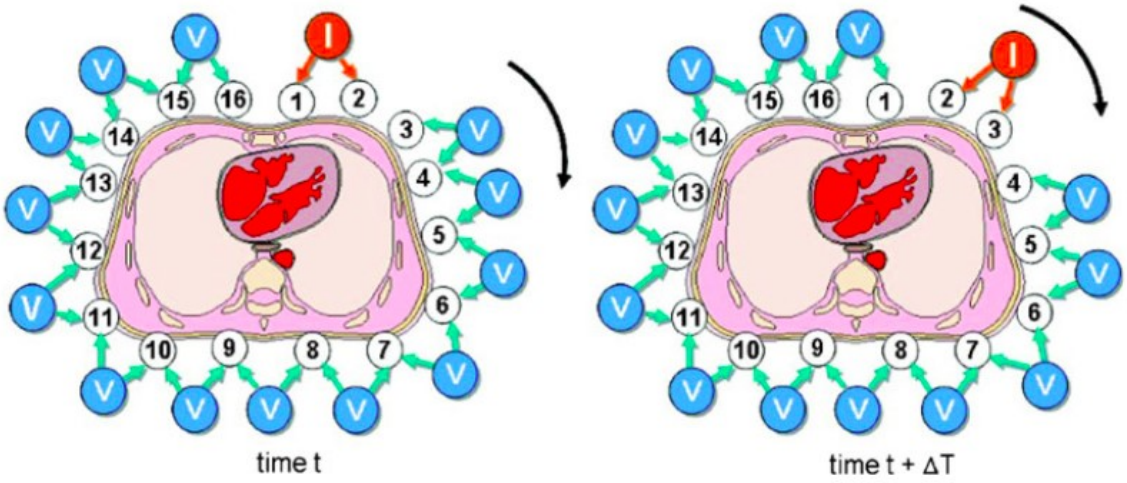

Figure 15. *The rotation of the current injection and the voltage measurement in EIT. (Leonhardt et al. 2012)*

The concept of *relative EIT* was first introduced by Barber et al. (1990) and later Hahn et al. (1995). The reason for the introduction of relative EIT was to overcome the difficulty of obtaining accurate *absolute EIT* images, which need detailed knowledge about geometry and absolute electrode positioning. In order to cancel most of the geometric artifacts common in absolute EIT images, in relative EIT the average impedance over a certain time period is subtracted from the actual impedance value. Thus, only impedance changes are visible and the absolute impedance values are lost.

The mathematical principle behind the image constructions is based on solving an inverse problem. Detailed explanation of the image construction and EIT can be found e.g. Scherzer (2010) and Bayford (2006). The EIT has various clinical applications including pulmonary and brain function measurements, which include presurgical assessment for epilepsy, diagnostics of stroke and intraventricular bleeding in preterm neonates (Bayford 2012; Leonhardt & Lachmann 2012). In the following section a few studies that utilized the ETI for determining the conductivity of brain tissue, are introduced.

Gonçalves et al. (2003a) measured the equivalent electrical resistivity of skull and brain by using two different methods based on spherical head models. The first method utilizes the principles of EIT and a current at 60 Hz. The average obtained resistivity of six subjects for the brain was 3.05 Ωm and for the skull 203.55 Ωm. As the other method they recorded the evoked somatosensory cortical responses simultaneously with

magnetoencephalography (MEG) and electroencephalography (EEG). They estimated the equivalent electrical resistivities through a combined analysis of the evoked responses. MEG/EEG system was used to record the data generated from the stimulation of the median nerve. The stimulus was set at 2 Hz and the duration at 0.2 ms. The obtained resistivities were 2.34 Ωm for the brain and 161.85 Ωm for the skull.

Gonçalves et al. (2003b) published another article on measuring the resistivities with EIT, but this time a realistic head model was used instead of a spherical one. The head model consisted of three isotropic and homogenous compartments: scalp, skull and brain. The MRI scans of each of the six patients were used to obtain the shapes of the three compartments. The classical boundary element method (BEM) was used to solve the forward problem of EIT. The frequency of the injected current was 60 Hz. The obtained average resistivities were 3.01 Ωm for the brain and 122.30 Ωm for the skull. Thus, the average skull to brain -ratio was 42.

2.5.3. Ex-vivo studies

Schmid et al. (2003a) measured the brain conductivity on 20 human brains post mortem. The measurements were performed right after excising the brain during a routine autopsy, which was performed within ten hours after death. A vector network analyzer and an open ended coaxial probe were used as the measurement system. They measured the conductivity from four specific places on the left and right temporal lobe in the frequency range of 800 to 2,450 MHz. The arachnoidea and pia mater were kept intact during the measurements. The mean post mortal tissue age was 6.7 hours, mean tissue temperature was 21.35 °C and average age of the patients was 70.4 years. The obtained mean conductivity for grey matter was 1.17 S/m at 900 MHz and 1.64 S/m at 1800 MHz or 0.85 Ωm and 0.61 Ωm respectively.

Akhtari et al. (2006) measured the conductivity of freshly excised neocortex and subcortical white matter in the frequency range from 5 to 1005 Hz in 21 epilepsy surgery patients with a four-electrode technique. A detailed description of the measurement setup can be found in their article (Akhtari et al. 2006). The conductivity results averaged with the respect to all frequencies and current densities ranged from 0.0668 to 0.145 S/m with an average of 0.0924 S/m or 10.8 Ωm and SD of 0.0216. The conductivity results of each patient at different frequencies are plotted in Figure 16. In addition, the figure shows the increase in conductivity when the frequency increases.

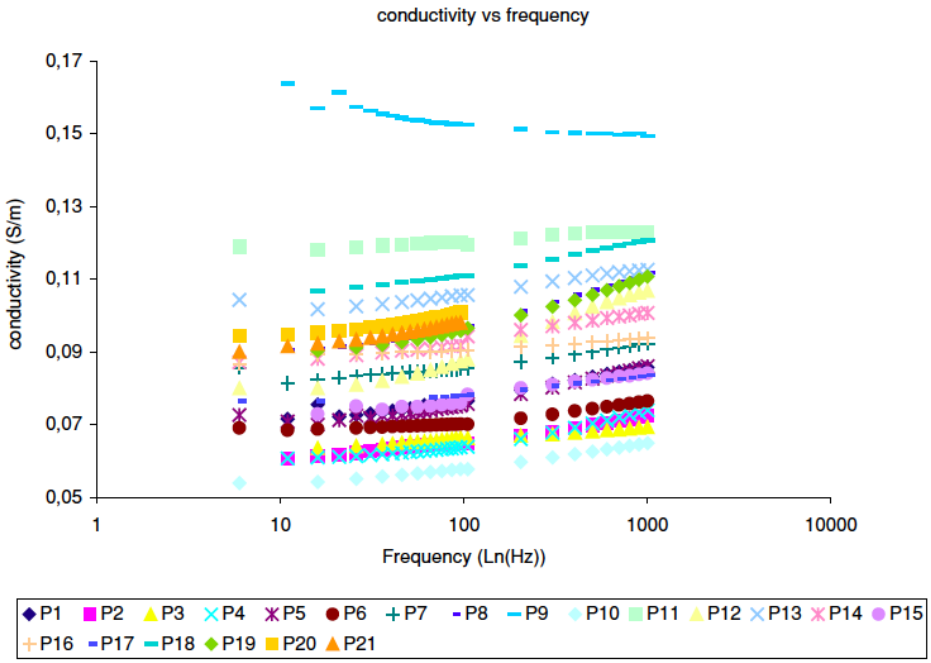

Figure 16. *The conductivity values at different frequencies. It should be noted that the tissue sample of patient number 18 was severely diseased compared to the samples of other patients. (Akhtari et al. 2006)*

Akhtari et al. (2010) continued their research on brain tissue conductivity with 15 pediatric epilepsy surgery patients. They measured conductivities perpendicular and parallel to pia matter of neocortex and subcortical white matter of freshly excised brains. They used the same measurement set up and frequency range as in their previous article. According to their study the average conductivities parallel and perpendicular to the pia mater differed by 243 % from one patient to another. Average parallel and perpendicular conductivities were 0.104 ± 0.016 S/m and 0.107 ± 0.021 respectively. The overall average conductivity was 0.10 ± 0.01 S/m. According to their study, patients with cortical dysplasia had lower conductivities compared to those without dysplasia.

Akhtari et al. (2016) measured the conductivity of freshly excised brain tissues from 24 pediatric epilepsy surgery patients. They again measured the conductivities in parallel and perpendicular to pia mater at low frequencies ($<10^3$) with the same technique as in their previous publications discussed earlier. The conductivity ranged from 0.05 S/m to 0.24 S/m and the average conductivity was 0.12 S/m or 8.33 Ωm. Their results indicate that the conductivity of the samples was basically isotropic, since the correlation between the parallel and perpendicular results was very high. They also measured the in-vivo diffusion-MRI of the hydrogen nuclei of the water molecules in the tissue sample areas before they were excised. A comparison between the conductivity and diffusion-MRI results indicated that the differences between the conductivity values of the tissue samples are mainly due to differences of their densities of solvated sodium

cations. Thus, by measuring the local density of sodium ions in the brain tissue, a reasonable estimate of the local conductivity could be obtained.

2.5.4. MRI utilized in conductivity measurements

Sekino et al. (2003) used a method based on diffusion-weighted MRI (4.7 T) to obtain conductivity tensor images of rat brain. The obtained mean conductivities for corpus callosum and cortex were 0.018 S/m or 55.6 Ωm and 0.014 S/m or 71.4 Ωm respectively. High level of anisotropy was exhibited in the corpus callosum.

Sekino et al. (2005) used 1.5 T MRI to obtain the spatial distribution of anisotropic conductivity of the human brain. They conducted the measurement on five healthy subjects. The conductivity of the grey matter showed no dependence on measurement direction, in turn the conductivity of the white matter exhibited high anisotropy. The obtained mean conductivity values were 0.060 ± 0.006 S/m, 0.077 ± 0.004 S/m and 0.097 ± 0.011 S/m for the putamen, the internal capsule and the corpus callosum respectively. The conductivity parallel to the neuronal fibers was higher than that in the perpendicular direction in the internal capsule and corpus callosum.

Sekino et al. (2009) obtained low frequency conductivity tensor maps of ten rat brains by using 4.7 T diffusion MRI and the signal attenuations were measured with stimulated echo acquisition mode sequence. The obtained mean conductivities of the cortex and corpus callosum were 0.52 S/m and 0.62 S/m respectively.

2.5.5. Animal studies

Schmid et al. (2003b) studied the postmortem changes of the dielectric properties of gray matter on ten pigs with a dielectric probe and a vector network analyzer. They kept the animals in stable anesthesia and then euthanized them by an intravenous injection of hypertonic potassium chloride. They measured the conductivity on the surface of intact arachnoid with frequency range of 800-1900 MHz. They used a special heating device to avoid contact cooling of the brain tissue thus maintaining the normal tissue temperature of a pig (38°C). They measured the conductivity at the time of death and 15 and 60 minutes after death. The obtained conductivity values are presented in Table 1.

Table 1. *The obtained conductivity values measured at the time of death, 15 minutes and 60 minutes after death at 900 and 1800 MHz. (Schmid 2003b)*

Frequency (MHz)	**Conductivity values obtained at certain time after death (S/m)**		
	0 min	15 min	60 min
900	1.28	1.15	1.09
1800	1.67	1.55	1.50

They discovered that within the first hour after death the mean equivalent conductivity of grey matter decreased about 15% at 900 MHz and 11% at 1800 MHz. The permittivity showed no dramatic changes and was almost frequency independent.

2.6. Impedances of brain tissues found in literature

A literature review was made and all the brain tissue resistivity values are compiled on the next page in Table 2.

Table 2. *Brain tissue resistivity values found in literature.*

Study	Grey matter (Ωm)	White matter (Ωm)	CSF (Ωm)
Latikka et al. 2001	3.51 (50 kHz)	3.91 (50 kHz)	0.80 (50 kHz)
Gonçalves et al. 2003	3.5 (whole brain, EIT-method) 2.34 (whole brain, SEF/SEP method)		-
Schmid et al. 2003a	0.85 (900MHz) 0.61 (1800MHz)	-	-
Koessler et al. 2016	3.78 (50 kHz)	5.24 (50 kHz)	-
Schmid et al. 2003b	0.78 (900MHz) 0.60 (1800MHz)	-	-
Akhtari et al. 2006	10.8 (whole brain, 5-1005 Hz)		-
Akhtari et al. 2010	10.0 (whole brain, 5-1005 Hz)		-
Akhtari et al. 2016	8.33 (whole brain, $<10^3$ Hz)		-
Sekino et al. 2003	71.4 (MRI)	55.6 (MRI)	-
Sekino et al. 2005	16.6 (MRI)	13.0 (internal capsule, MRI) 10.3 (corpus callosum, MRI)	-
Sekino et al. 2009	1.92 (MRI)	1.61 (corpus callosum, MRI)	-

3. MATERIALS AND METHODS

In this chapter a method for obtaining brain tissue impedances with deep brain stimulation electrodes is introduced.

3.1. Patients

These measurements can be conducted on a patients undergoing implantation of deep brain stimulation electrodes. The wider the patient selection, the diverse are the results. In other words, if all the subjects have for example Parkinson's, the majority of the conductivity results would be from the vicinity of the STN, since STN is the most common target used in the treatment of Parkinson's. Thus, by expanding the patient selection to patients with e.g. epilepsy and dystonia, the conductivity results would be obtained from more diverse locations in the brain. A minor delay, only few minutes, is caused before the implantation. However, no additional harm except the short delay is caused to the patient due to the measurements.

3.2. Recording device

Medtronic DBS N'Vision (Figure 17) is used as the recording device for these measurements. N'vision is a clinician programmer for drug delivery and neurostimulation. The programmer is battery-operated, 22x10x4 cm in size and is equipped with 240x640 pixel touchscreen display in addition to telemetry head for device programming and an infrared port for connecting to a printer.

Figure 17. *Medtronic DBS N'Vision (Medtronic website)*

3.3. Electrodes

There are two lead models compatible with the recording device, model 3387 and 3389. Both models contain four cylindrical platinum-iridium electrodes numbered 0-3 in the distal tip (Figure 18).

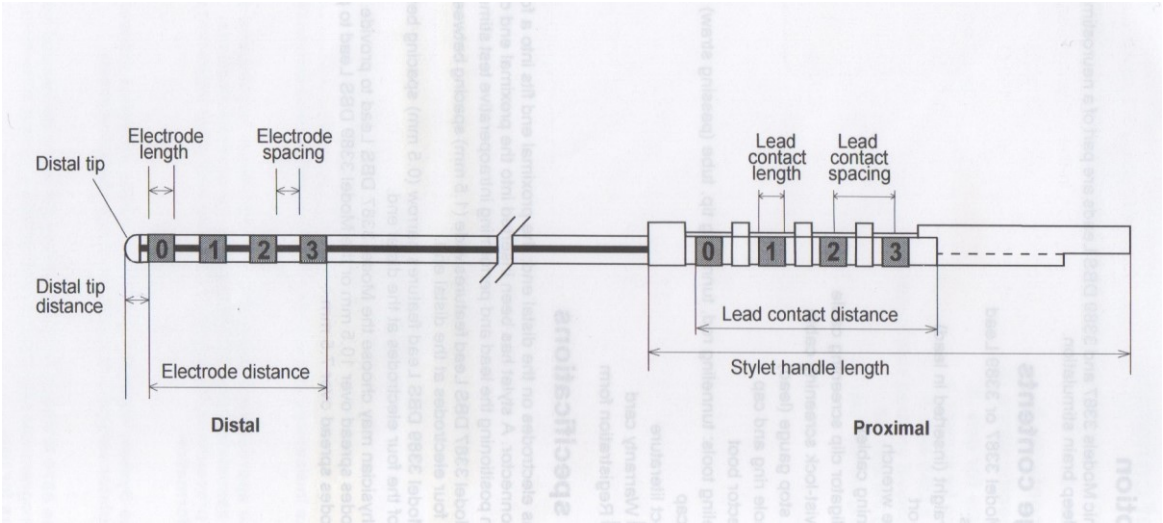

Figure 18. *The structure of the lead. (Medtronic Implant manual 2010)*

The only difference between the lead models is the electrode spacing and thus, the electrode distance. The specifications of the lead models are presented in Table 3.

Table 3. *The specifications of the lead models 3387 and 3389. (Medtronic Implant manual 2010)*

Description	Model 3387	Model 3389
Connector	Quadripolar, in-line	Quadripolar, in-line
Shape	Straight	Straight
Diameter	1.27 mm	1.27 mm
Length	10-50 cm	10-50 cm
Electrode length	1.5 mm	1.5 mm
Electrode spacing	1.5 mm	0.5 mm
Electrode distance	10.5 mm	7.5 mm
Distal tip distance	1.5 mm	1.5 mm

The electrode configurations for deep brain stimulation are either bipolar or monopolar. In monopolar configuration the pulse generator or the programmer act as the positive pole and electrode as the negative, while in the bipolar other electrodes act as the positive pole and others as the negative as seen in Figure 19.

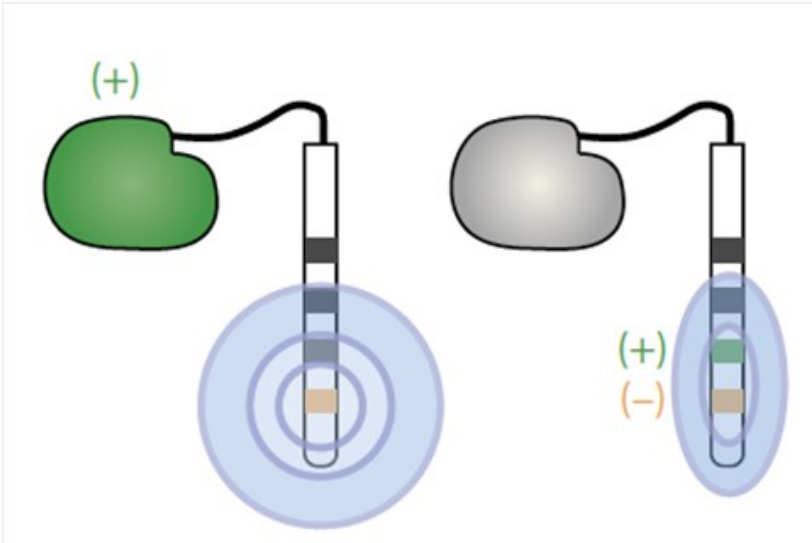

Figure 19. *The monopolar (left) and bipolar (right) electrode configurations. (Pekkonen 2013)*

With bipolar configuration the electric field is smaller compared to unipolar and causes less side effects. However, monopolar stimulation activates a larger field thus, resulting

a better response compared to bipolar. Several electrodes can be active simultaneously, which increases the power consumption.

3.4. Measurement principle

N'Vision has a preprogrammed Electrode Impedance Measurement –option, which is used to check the integrity of the lead after implantation. This option measures the resistance of the leads, extensions and body tissue with 0.4 mA current, pulse width of 80 μs and frequency of 100 Hz. Measurements that are within the normal limits indicate that the conduction pathways are intact. Impedance values less than 250 ohms indicate a possible short circuit, whilst values greater than 4000 ohms during bipolar measurement indicate a possible open circuit. (Medtronic N'Vision manual 2011)

The Electrode Impedance Measurement measures the impedance with six different combinations of electrodes. Thus, it is bipolar and the polarity (positive, negative, off) of each of the electrode varies depending on the electrode combination (Table 4). The electrode is placed in different locations for each patient, thus the brain matter and structures in contact with each lead differ among patients. (Medtronic N'Vision manual 2011) However, the neurosurgeon should be able to locate each electrode with the aid of MRI and CT- scan and determine whether the electrode is in contact with grey or white matter.

Table 4. *The different electrode combinations*

Electrode combinations
0 & 1
0 & 2
0 & 3
1 & 2
1 & 3
2 & 3

3.5. Calibration and testing

The calibration and testing consists of measurements done both in a laboratory and in the OR during the surgery.

3.5.1. In the laboratory

The goal of the laboratory tests is to examine how N'vision and the leads perform when the impedance increases and how the impedance values obtained with N'vision correlates to the real values or *the golden standard*. Since there are two lead models, the following tests should be performed on both of them. To separate the leads used in the laboratory from the leads that are implanted, these laboratory leads are referred as calibration leads from now on.

Every patient receives a brand-new lead and some difference is to be expected amongst the leads e.g. in their impedances, some kind of a correlation has to be made between the leads in order to compare the impedance results. An isotonic solution of several salts dissolved in water known as the *Ringer's solution* is used to obtain this correlation. The impedance of Ringer's solution as a function of temperature is measured with the calibration electrode and then plotted. 20-26 °C is a sufficient temperature range, since the measurements with the Ringer's solution in the OR are performed around room temperature.

The electrodes are purely resistive thus the impedance of the calibration electrode can be measured with a multimeter. The measurement is done by placing the positive probe on the electrode in the proximal end and the negative probe on the same numbered electrode in the distal end. This is repeated for each of the four electrodes (Figure 18).

Other measurements are performed with salt and water in order to check the linearity of the N'Vision i.e. how the N'Vision works when the conductivity increases. A precalibrated conductivity meter is used as the golden standard. Thus, the conductivity results obtained with the conductivity meter are considered as the real and correct conductivity values. For example one liter of water is placed in a plastic container and table salt is added to it. The conductivity is then measured with the conductivity meter and the impedance with the N'Vision. To increase the conductivity, table salt is added and the measurements are repeated until the operation range of the electrodes, 300 - 4000 Ω, is covered. A sufficient number of measurements should be performed within the range of interest in order to plot an accurate graph of the relation between the conductivity meter and the N'Vision. The procedures before the plotting are explained later in the calculations –section.

3.5.2. In the OR during surgery

As mentioned earlier, every patient receives a brand new lead, thus the impedance of these new electrodes should be checked before implantation in every surgery. By immersing the lead in Ringer's solution in a sterile and nonmetallic dish or container and measuring its impedance, comparable results will be obtained in every surgery. The temperature of the Ringer solution must be measured and it is best if the temperature is

very close to room temperature in order to facilitate the comparison of the results. Since the measurements must be done in a sterile manner, the immersing of the lead is best to do right before implantation to avoid any contamination and the temperature is measured with a thermometer right after the impedance measurement. The measurement takes only a few minutes, thus no major delays are caused to the surgery.

3.6. Calculations to obtain the actual brain tissue impedance values

The temperature of the Ringer's solution used in the OR may vary and there certainly is some standard deviation in the electrode impedance amongst leads. In the laboratory, the impedance of the Ringer's solution as a function of temperature is measured with the calibration electrode and the results then plotted. The impedance of the calibration electrode in the temperature in which the measurement was done in the OR is checked from the graph. The difference between the impedance of the new electrode and the calibration electrode in this temperature is then determined and is referred as *Δ(electrode impedance)* from now on. This procedure links the all the new leads to the calibration lead in a way that the impedance results can be compared amongst the leads, since it is impossible to calibrate all the new leads due to unavoidable contamination caused by the methods used.

In order to plot an accurate correlation graph between the N'Vision and the conductivity meter, the electrode impedance of each electrode combination and *Δ(electrode impedance*) of that combination must be subtracted from the results. For example, if the combination is 0 & 1, then impedances of both electrodes 0 and 1 must be subtracted in addition to the difference between the impedance value of that combination of the calibration electrode and the implanted lead. This procedure is then repeated to the rest of the combinations. The resistance of the conductor of the N'Vision is > 20 Ω, thus it is negligible and so is the resistance of the conductor of the conductivity meter.

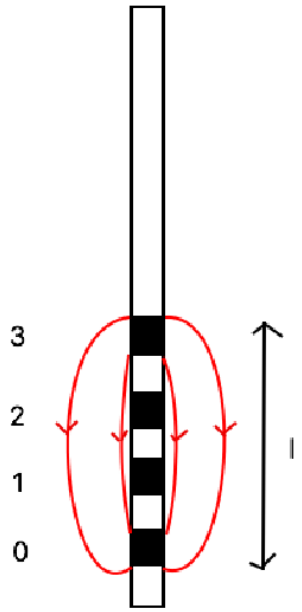

Figure 20. *The path of the current in the medium and the length l of the combination 0 & 3.*

For these measurements, the impedance results obtained with the N'Vision have to be converted to conductivity values. The path the current passes through the medium between the electrodes can be considered as a cylinder from one electrode to another as seen in Figure 20. If the tissue between the electrodes is closed, the conversion can be done by using the following formula

$$\sigma = \frac{l}{Z * A},$$

where A is the area of the current path and l the is the length between the electrodes. The length depends on the electrode combination and the lead model. The length between each electrode combination is calculated and presented for both lead models in Table 5.

Table 5. *The lengths between the electrode combinations.*

Electrode combination	The length between the electrode combination (mm)	
	Model 3387	Model 3389
0 & 1	4.5	3.5
0 & 2	7.5	5.5
0 & 3	10.5	7.5
1 & 2	4.5	3.5
1 & 3	7.5	5.5
2 & 3	4.5	3.5

The area is the same in both models since the diameter and electrode length are equal in both models. Thus, the area of the current path is

$$A = x * \pi * d = 5.98473\ \mu m^2,$$

where x is the width of the electrode (1.5 mm) and d is the diameter of the lead (1.27 mm). This gives the maximum estimate for the conductivity. In reality the conductivity values should be calibrated by using Ringer solutions with known conductivities.

3.7. Ethical issues

In order to conduct the measurements on living patients, permission of the Ethics Committee of the Hospital District must be applied.

4. DISCUSSION

The intracerebral methods on live patients have several advantages compared to extracranial methods. The attenuating effect of the skull and meninges is removed when the measurements are done from the actual brain tissue. The intracerebral methods avoid the uncertainties related to solving the inverse problem and modeling of the head that are the major constraints in EIT.

The dielectric properties of brain tissue depend on the temperature thus intracerebrally measured the optimal temperature is achieved. The resistivity of brain tissue increases after death (Schmid 2003b; Gamba & Delpy 1998), thus post mortem resistivity measurements e.g. from tissue sample, do not provide reliable data.

The method Latikka (1999; 2001) used is able to measure the conductivity of the tissue along the entire path through which the needle electrode is inserted. However, the measurements can only be performed from the surgical path thus the conductivity values obtained only describe the certain part of the brain in certain direction. The fact that brain tissue is anisotropic i.e. the conductivity depends on the measurement direction brings uncertainties and difficulties in the conductivity measurement.

According to Latikka (2001) the tissue type in question was determined by the information offered by the MRI - and CT –scans of each patient. Since large number of the patients had tumors of some sort, the line between healthy tissue and tumor tissue was not always clear. The calibration of the recording device plays a major role in determining the accuracy of the conductivity results. A tiny mistake in the calibration process might affect greatly on the results. Other error sources in Latikka's measurement included bleeding, the saline used for washing and the leakage of CSF to the measurement site. However, all these factors are extremely hard to avoid when dealing with real live brain tissue.

The advantages of the method introduced in this thesis include the easy execution of the measurement, since the preprogrammed electrode impedance measurement is performed in every installment of DBS electrodes to check their integrity. The measurements are done on a living brain tissue without the skull, the meninges and hopefully without the presence of tumors.

The disadvantages this method has are basically the same as the method designed by Latikka such as the tissue type can only be determined from the MRI – and CT – scans and the fact that the measurement environment is hard to control in case of e.g. bleeding

etc. In addition, the electrode is passed to the brain through a tiny metallic tube that is inserted to the brain according to exact coordinates. This metallic insertion tube makes it impossible to take measurements along the insertion pathway i.e. the measurements can only be performed in the electrodes target. The calibration of the recording device is the key to obtain accurate results also in this method, since the calibration method contains several calculations. The Ringer's solution measurement in the OR must be done using extreme caution to avoid contamination of the electrode being implanted. Thus, a sterile nonmetallic dish must be used with brand new Ringer's solution in every surgery.

The fact that in this method the shape of the current path in the medium is modeled as a cylinder with a same shape or thickness throughout the whole distance might distort the actual conductivity values. This assumption is very rough and it will not provide accurate results. Therefore, before the brain tissue measurement the conductivity should be somehow measured from a known reference e.g. Ringer solution on the surface of the brain.

However, the method designed in this thesis offers a possibility to measure the brain tissue in other parameter values than the ones that are preprogrammed to check the lead integrity. In other words, the measurements can be done e.g. with different set of frequencies and currents to determine how the tissue behaves.

Considering for example the fact that the typical frequency used in DBS for Parkinson's is around 130 Hz as mentioned earlier, the frequency used in the measurement of brain tissue resistivity should be close to the values used in the applications, where the knowledge of the dielectric properties of the brain tissue play a major role. Also the different dispersions described earlier affect the results, since the resistivity decreases rapidly in certain frequencies. Schmid et al. (2003a) used the range from 800 to 2,450 MHz, which is immensely above the frequency used in DBS. They also measured the conductivities on dissected brain with arachnoidea still intact, thus is extremely hard to evaluate how closely their results corresponds to in vivo values. On the other hand, they were able to measure the conductivity from several different sites of the brain, which is not yet possible in vivo with the current methods.

The EIT is a relatively new and promising imaging technique for example continuous bedside monitoring of impedance changes. It is a non-invasive, portable and radiation free real-time imaging modality, which is easy to use and harmless to the patient. It has high temporal resolution (13-50 frames/s) and image quality. The costs of EIT system are relatively low. (Bayford 2012; Leonhardt & Lachmann 2012) Studies where actual conductivity values have been obtained with EIT are sparse, but e.g. Gonçalves (2003a &2003b) has published actual values.

The spatial resolution of EIT is significantly lower than the temporal resolution and at best is limited to the distance between the electrodes. The inverse problem brings uncertainties and the presence of artifacts, where they are not expected, introduces uncertainty in a clinical setting. Sources of artifacts include electrode placement both in the forward model and subject, inadequate modeling of the electrodes in the forward model, subject movement during measurement and geometric non-compliance between the forward model and the subject. (Bayford 2012; Leonhardt & Lachmann 2012)

The MRI-based method Sekino used in his studies (2003; 2005; 2006) proved to obtain notably higher conductivity results compared to other methods. This is an indication that there is still a lot of development and improvement to be done before MRI –based methods can be used in brain tissue conductivity value estimation. However, this methods seems to be a promising tool in brain impedance distribution imaging.

The future research should focus on controlling the brain tissue environment during conductivity measurements, since changes in temperature, chemical composition, stress level and oxygen concentration have significant effect on the conductivity. Blood has lower impedance than cortex so changes in blood volume and flow during brain activity changes the conductivity of the brain tissue. Brain is heavily vascularized thus the effect of blood seems inevitable at this point. The conductivity depends on the measurement direction, thus anisotropy is another issue, which should be further investigated. Also the individual variability of conductivity and the variability of conductivity in different points in the brain should be investigated.

5. CONCLUSIONS

The brain tissue conductivity values are very limited and the values vary considerably. Only a single study has been conducted (Latikka 2001), where they measured the conductivity on living patients in an OR. The measurements are very challenging to perform with the current DBS hardware. Nevertheless, we believe that the measurements can be performed with the method presented in this thesis.

REFERENCES

Akhtari, M., Salamon, N., Duncan, R., Fried, I., & Mathern, G. W. (2006). Electrical conductivities of the freshly excised cerebral cortex in epilepsy surgery patients; correlation with pathology, seizure duration, and diffusion tensor imaging. Brain topography, 18(4), 281-290.

Akhtari, M., Mandelkern, M., Bui, D., Salamon, N., Vinters, H. V., & Mathern, G. W. (2010). Variable anisotropic brain electrical conductivities in epileptogenic foci. Brain topography, 23(3), 292-300.

Akhtari, M., Emin, D., Ellingson, B. M., Woodworth, D., Frew, A., & Mathern, G. W. (2016). Measuring the local electrical conductivity of human brain tissue. Journal of Applied Physics, 119(6), 064701.

Barber, D. C., Brown, B. H., & Freeston, I. L. (1984). Imaging spatial distributions of resistivity using applied potential tomography—APT. In Information Processing in Medical Imaging (pp. 446-462). Springer Netherlands.

Barber, D. C. (1990). Quantification in impedance imaging. Clinical Physics and Physiological Measurement, 11(4A), 45.

Bayford, R. H. (2006). Bioimpedance tomography (electrical impedance tomography). Annu. Rev. Biomed. Eng., 8, 63-91.

Bayford, R., & Tizzard, A. (2012). Bioimpedance imaging: an overview of potential clinical applications. Analyst, 137(20), 4635-4643.

Bear, M. F., Connors, B. W., & Paradiso, M. A. (2016). Neuroscience: Exploring the brain (4th ed.). Philadelphia: Wolters Kluwer.

Bronte- Stewart, H., Taira, T., Valldeoriola, F., Merello, M., Marks, W. J., Albanese, A., & Bressman, S. (2011). Inclusion and exclusion criteria for DBS in dystonia. Movement disorders, 26(S1).

Bronzino, J. D. (1995). The biomedical engineering handbook. Boca Raton, Fla: CRC Press.

Cole, K. S., & Cole, R. H. (1941). Dispersion and absorption in dielectrics I. Alternating current characteristics. The Journal of chemical physics, 9(4), 341-351.

DBS Lead Kit for deep brain stimulation 3387 & 3389 (2010), Implant manual, Medtronic, 212 p.

Follett, K. A., Weaver, F. M., Stern, M., Hur, K., Harris, C. L., Luo, P., ... & Pahwa, R. (2010). Pallidal versus subthalamic deep-brain stimulation for Parkinson's disease. New England Journal of Medicine, 362(22), 2077-2091.

Gamba, H. R., & Delpy, D. T. (1998). Measurement of electrical current density distribution within the tissues of the head by magnetic resonance imaging. Medical and Biological Engineering and Computing, 36(2), 165-170.

Gonçalves, S., de Munck, J. C., Verbunt, J. P., Heethaar, R. M., & da Silva, F. H. (2003a). In vivo measurement of the brain and skull resistivities using an EIT-based method and the combined analysis of SEF/SEP data. IEEE transactions on bio-medical engineering, 50(9), 1124-1128.

Gonçalves, S. I., de Munck, J. C., Verbunt, J. P., Bijma, F., Heethaar, R. M., & da Silva, F. L. (2003b). In vivo measurement of the brain and skull resistivities using an EIT-based method and realistic models for the head. IEEE Transactions on Biomedical Engineering, 50(6), 754-767.

Hahn, G., Sipinkova, I., Baisch, F., & Hellige, G. (1995). Changes in the thoracic impedance distribution under different ventilatory conditions. Physiological measurement, 16(3A), A161.

Hall, J. E. (2016). Guyton and hall textbook of medical physiology (13th ed.). Philadelphia: Elsevier.

Hamani, C., McAndrews, M. P., Cohn, M., Oh, M., Zumsteg, D., Shapiro, C. M., ... & Lozano, A. M. (2008). Memory enhancement induced by hypothalamic/fornix deep brain stimulation. Annals of neurology, 63(1), 119-123.

Hartikainen M. (2015) Syväaivostimulaatiohoidon vaikutus tiedonkäsittely- ja tunnetoimintoihin.

Henderson, R. P., & Webster, J. G. (1978). An impedance camera for spatially specific measurements of the thorax. IEEE Transactions on Biomedical Engineering, (3), 250-254. Lyons MK. Deep brain stimulation: current and future clinical applications. Mayo Clin Proc 2011;86(7):662-72. PubMed

Krack, P., Hariz, M. I., Baunez, C., Guridi, J., & Obeso, J. A. (2010). Deep brain stimulation: from neurology to psychiatry?. Trends in neurosciences, 33(10), 474-484.

Latikka, J. (1999) Determination of conductivities for head tissues, Master of Science Thesis, Tampere University of Technology. 65 p.

Latikka, J., Kuurne, T., & Eskola, H. (2001). Conductivity of living intracranial tissues. Physics in medicine and biology, 46(6), 1611.

Leonhardt, S., & Lachmann, B. (2012). Electrical impedance tomography: the holy grail of ventilation and perfusion monitoring?. Intensive care medicine, 38(12), 1917-1929.

Lyons KE, Pahwa R. (2008). Thalamic deep brain stimulation. In Deep brain stimulation in neurological and psychiatric disorders (pp. 83-98). Humana Press.

Martinsen, O. G., & Grimnes, S. (2011). Bioimpedance and bioelectricity basics. Academic press.

N'Vision clinician programmer with software (2011), Device manual, Medtronic, 110 p.

Pekkonen, E. (2013). Syväaivostimulaatio neurologisissa sairauksissa. Duodecim, 129, 481-488.

Plonsey, R., & Barr, R. C. (2007). Bioelectricity: a quantitative approach. Springer Science & Business Media.

Purves, D. (2012). neuroscience (5.th ed.). Sunderland, Mass: Sinauer Associates.

Reilly, J. P., & Antoni, H. (1992). Electrical stimulation and electropathology. Cambridge University Press.

Ross, M. H., & Pawlina, W. (2016). Histology: A text and atlas (7th ed.). Philadelphia: Wolters Kluwer Health.

Scherzer, O. (Ed.). (2010). Handbook of mathematical methods in imaging. Springer Science & Business Media.

Schmid, G., Neubauer, G., & Mazal, P. R. (2003a). Dielectric properties of human brain tissue measured less than 10 h postmortem at frequencies from 800 to 2450 MHz. Bioelectromagnetics, 24(6), p. 423-430.

Schmid, G., Neubauer, G., Illievich, U. M., & Alesch, F. (2003b). Dielectric properties of porcine brain tissue in the transition from life to death at frequencies from 800 to 1900 MHz. Bioelectromagnetics, 24(6), 413-422.

Schuenke, M., Schulte, E., & Schumacher, U. (2011). Thieme atlas of anatomy: Head and neuroanatomy. New York;Stuttgart;: Thieme.

Schwan, H. P. (1994). Electrical properties of tissues and cell suspensions: Mechanisms and models. Paper presented at the , 1 A70-A71 vol.1. doi:10.1109/IEMBS.1994.412155

Sekino, M., Yamaguchi, K., Iriguchi, N., & Ueno, S. (2003). Conductivity tensor imaging of the brain using diffusion-weighted magnetic resonance imaging. Journal of applied physics, 93(10), 6730-6732.

Sekino, M., Inoue, Y., & Ueno, S. (2005). Magnetic resonance imaging of electrical conductivity in the human brain. IEEE transactions on magnetics, 41(10), 4203-4205.

Sekino, M., Ohsaki, H., Yamaguchi- Sekino, S., Iriguchi, N., & Ueno, S. (2009). Low-frequency conductivity tensor of rat brain tissues inferred from diffusion MRI. Bioelectromagnetics, 30(6), 489-499.

Siddiqui, M. S., Ellis, T., Tatter, S. S., Foote, K. D., & Okun, M. S. (2008). Deep brain stimulation: patient selection in Parkinson's disease, other movement disorders, and neuropsychiatric disorders. In Deep brain stimulation in neurological and psychiatric disorders (pp. 83-98). Humana Press.

Tampere University Hospital. Syväaivostimulaatio (DBS). Available: http://www.pshp.fi/fi-FI/Palvelut/Neuroalat/Neurokirurgia/Syvaaivostimulaatio_DBS *(referred 17.9.2017)*

Vidailhet M, Grabli D, Roze E. (2008). Deep brain stimulation in dystonia. In Deep brain stimulation in neurological and psychiatric disorders (pp. 83-98). Humana Press.